

Eulerian bias and the galaxy density field

R.G. Mann,^{1,2,3} J.A. Peacock⁴ and A.F. Heavens¹

¹*Institute for Astronomy, Department of Physics and Astronomy, University of Edinburgh, Blackford Hill, Edinburgh EH9 3HJ*

²*Astronomy Unit, Queen Mary and Westfield College, Mile End Road, London E1 4NS*

³*Present Address: Astrophysics Group, Blackett Laboratory, Imperial College, Prince Consort Road, London SW7 2BZ*

⁴*Royal Observatory, Blackford Hill, Edinburgh, EH9 3HJ*

28 June 2018

ABSTRACT

We investigate the effects on cosmological clustering statistics of empirical biasing, where the galaxy distribution is a local transformation of the present-day Eulerian density field. The effects of the suppression of galaxy numbers in voids, and their enhancement in regions of high density, are considered, independently and in combination. We compare results from numerical simulations with the predictions of simple analytic models. We find that the bias is generally scale-dependent, so that the shape of the galaxy power spectrum differs from that of the underlying mass distribution. The degree of bias is always a monotonic function of scale, tending to an asymptotic value on scales where the density fluctuations are linear. The scale dependence is often rather weak, with many reasonable prescriptions giving a bias which is nearly independent of scale.

We have investigated whether such an Eulerian bias can reconcile a range of theoretical power spectra with the twin requirements of fitting the galaxy power spectrum and reproducing the observed mass-to-light ratios in clusters. It is not possible to satisfy these constraints for any member of the family of CDM-like power spectra in an Einstein - de Sitter universe when normalised to match *COBE* on large scales and galaxy cluster abundances on intermediate scales. We discuss what modifications of the mass power spectrum might produce agreement with the observational data.

Key words: Galaxies: clustering; cosmology: large-scale structure of Universe.

1 INTRODUCTION

The great advances in observational cosmology during the past decade have provided a wealth of new data on galaxy clustering. These results facilitate a phenomenological approach to the study of large-scale structure, in which the mass power spectrum is reconstructed directly from the observed clustering statistics (e.g. Peacock & Dodds 1994, PD94). This method is complementary to the hitherto conventional technique of judging a pet cosmogony on the basis of its predictions for a series of observationally-determined quantities, and has some advantages so long as no specific model appears capable of accounting for the full set of observational data.

There is, however, a fundamental problem with both the empirical and the a priori approaches to large-scale structure. The linear mass power spectrum that one deduces from the observed clustering depends on, and may be very sensitive to, an assumed relationship between the distributions of mass and galaxies in the Universe, and ignorance of the detailed processes through which galaxies form leaves this relationship poorly constrained. Different classes of galaxy

are observed to cluster differently (see, e.g., the compilation by PD94), implying that at least some galaxies are biased and do not directly trace the mass distribution. Bias is also required by advocates of an Einstein - de Sitter universe, to reconcile observed cluster M/L values that imply $\Omega \simeq 0.2$ with the assumed critical density. In the absence of a complete understanding of galaxy formation and evolution, large-scale structure theorists are left to model bias in as plausible a manner as they can.

Many such attempts have used the high-peak bias method (Davis et al. 1985; Bardeen et al. 1986, BBKS). We will term this a *Lagrangian* bias scheme, since it identifies the sites of nascent objects (galaxies or clusters) with peaks in the *initial* density field, smoothed on a scale appropriate to the mass of the objects under consideration. If the initial density field is Gaussian, then these peaks are more strongly clustered than the mass distribution as a whole, producing the desired bias. N -body simulations (e.g. Katz, Quinn & Gelb 1993) have revealed a poor correspondence between the particles found in galaxy halos selected at late times and those located at appropriate peaks in the initial density field, thus casting doubt on Lagrangian galaxy bias

prescriptions (although the work of Mo & White 1996 and Mo, Jing & White 1996 suggests Lagrangian bias may work statistically): this is not surprising, since the density field smoothed on the scale of galaxies is highly non-linear. For cluster-sized halos, however, Lagrangian bias may still be appropriate (Kaiser 1984; Cole & Kaiser 1989; Mann, Heavens & Peacock 1993), since their spatial distribution has undergone far less dynamical evolution.

In reality, galaxy formation must be more complex than this, involving a range of feedback mechanisms (Dekel & Rees 1987; Babul & White 1991). One might hope that all these issues would eventually be clarified by large numerical simulations which include a hydrodynamical treatment of baryons, as well as dissipationless dark matter, but such codes are in their infancy. An intriguing early result from one such code was the observation by Cen & Ostriker (1992; CO) of a tight correlation between the present-day (Eulerian) density field, ρ_m , and the local number density, ρ_g , of galaxies, formed using what those authors termed a ‘heuristic but plausible’ prescription, which creates a dissipationless protogalactic particle wherever the local baryonic component is sufficiently dense, rapidly cooling, contracting and Jeans unstable. Together with the observed uniformity of M/L values as a function of scale, these results motivate the general idea of *Eulerian* bias models, in which the galaxy number density at redshift zero is a function of the local value of the evolved mass density field. Some general aspects of such prescriptions were considered by Coles (1993), who deduced various important inequalities relating the mass and galaxy correlation functions in these models.

Our approach here is as follows. We make no assumptions concerning the physical processes that lead to bias, simply taking their overall effect to be a local transformation of the Eulerian density field, the principal features of which are the suppression of galaxy numbers in low-density regions and their enhancement in regions of high density. In Section 2 we outline the set of bias prescriptions combining these components which are to be studied here, using the combination of numerical and analytical methods described in Section 3, while Section 4 shows the effect of biasing CDM-like mass models by these methods. We focus on the question of the scale-dependence of the Fourier space bias parameter, $b(k)$, defined as the square root of the ratio of the galaxy and mass power spectra:

$$b(k) \equiv [\Delta_g^2(k)/\Delta_m^2(k)]^{1/2}, \quad (1)$$

where $\Delta_g^2(k)$ and $\Delta_m^2(k)$ are, respectively, the galaxy and mass power spectra. We employ the dimensionless form of the power spectrum, $\Delta^2(k)$, which is defined to be the variance per $\ln k$ [i.e. $\Delta^2(k) = d\sigma^2/d \ln k \propto k^3 P(k)$]. Our results indicate that $b(k)$ tends to a constant value on scales where the density field is linear, with only a weak tendency to change with scale for most reasonable bias prescriptions: we shall denote this asymptotic large-scale bias value by b_∞ .

Finally, we attempt to find a combination of a CDM-like mass model with a reasonable normalisation and a biasing prescription that can reproduce the observed power spectrum of galaxy clustering, while reconciling observed cluster M/L ratios with the critical density assumed in Einstein – de Sitter models. Details of this exercise and its results are given in Section 5, and are discussed in Section 6, where we also present the conclusions we draw from them.

2 EULERIAN BIAS

Our method is to choose some function to relate the galaxy and mass densities

$$\rho_g(\mathbf{x}) = f[\rho_m(\mathbf{x})], \quad (2)$$

and investigate its biasing properties: we assume that these density fields are defined on scales larger than that of individual galaxies. This is straightforward where the matter density is a continuous function, as is the case if there is an analytical model for the density field. The default model for the field at early times is a random Gaussian process, but this must be modified at late times when the field becomes non-linear. The simplest model which introduces the skewness necessary to avoid negative density is a lognormal density field (Coles & Jones 1991), for which the biased correlation function can be calculated analytically in many cases. These results are derived in the Appendix, and yield simple expressions for the linear bias in the limit of weak correlations: we shall quote these below as

$$b_{\text{LN}} \equiv \lim_{r \rightarrow \infty} \left[\frac{\xi_g(r)}{\xi_m(r)} \right]^{1/2}. \quad (3)$$

More realistic non-linear distributions are provided by N -body simulations, but here the density field is discrete, and must be smoothed in order to yield a continuous field. In practice, our approach is to weight the particles in the N -body simulation, depending on the local density of particles:

$$w = f[\rho_m]/\rho_m, \quad (4)$$

and to identify the resultant weighted particle density with the local galaxy density. Galaxies, of course, also form a discrete set of points, but we assume galaxies to be a Poisson sample of some continuous field, whose properties are to be estimated: we refer the reader to Coles (1993) for a discussion of the Poisson clustering model and local bias.

From the infinity of possible relationships between mass and galaxy density, we restrict ourselves to three parametric forms which are nevertheless sufficiently flexible to allow general conclusions to be drawn. The first two model the effects of increasing galaxy numbers in high density regions and suppressing them in voids, while the third is a functional form motivated by the numerical work of CO. The functional forms we consider are detailed in the next three sections.

It is important to note that these models quantify the relationship between the mass and galaxy distributions at redshift zero, rather than solely the process of galaxy formation itself: as emphasised by CO and others, the present-day distribution of galaxies reflects their movement since birth as much as the locations of those births. In particular, it may be difficult to predict the evolution of bias (Matarrese et al. 1997).

2.1 Power law bias

The first model we consider is power law bias:

$$\rho_g \propto \rho_m^B, \quad (5)$$

i.e. we apply a weight to each mass particle $\propto \rho_m^{B-1}$. With $B > 1$ equation (5) represents the enhancement of galaxy

numbers in high density regions. In the Appendix we show that the large-scale bias parameter for power law biasing of lognormal mass models is simply $b_{\text{LN}} = B$.

A reasonable choice for B would be the value required to decrease the mass-to-light ratio in clusters by a factor of about 5, sufficient to reconcile M/L measurements with an Einstein – de Sitter universe. If we take the centres of clusters to correspond to a mass overdensity of ~ 1000 , this suggests $B \simeq \ln(5000)/\ln(1000) = 1.23$, which is perhaps a surprisingly small degree of non-linearity. This is only a rough calculation, since it ignores the fact that the ρ^B transformation also scales the mean luminosity density. For the lognormal model in the Appendix, this correction can be calculated, leading to the slightly higher value of $B \simeq 1.4$. This argument is encouraging, since a small degree of bias is exactly what is needed on large scales. The linear fractional rms density contrast in $8 h^{-1}$ Mpc spheres is about 0.9, whereas the abundance of rich clusters suggests a figure of $0.5 - 0.6$ if $\Omega = 1$ (White, Efstathiou & Frenk 1993); a linear bias of about 1.5 is thus required.

2.2 Censoring bias

The next prescription we study is censoring, in which we assume that galaxies are not found in regions where the local mass density falls below a certain value, $\tilde{\rho}_m$: this represents both the migration of galaxies from underdense regions and the possibility that the galaxy formation process features some density threshold, below which galaxies cannot have formed by the present. In the absence of other bias, this is the ‘weighted bias’ model of Catelan et al. (1994), but it may readily be combined with power law bias, to yield a model where galaxy numbers are enhanced in high density regions and simultaneously suppressed in regions of low density:

$$\rho_g \propto \begin{cases} \rho_m^B & \text{if } \rho_m \geq \tilde{\rho}_m \\ 0 & \text{otherwise.} \end{cases} \quad (6)$$

In the lognormal approximation the large-scale bias for this model takes the form

$$b_{\text{LN}} = B + \frac{\sqrt{2/\pi} e^{-(\nu-B\sigma)^2/2}}{\sigma \left[1 - \text{erf} \left(\frac{\nu-B\sigma}{\sqrt{2}} \right) \right]}. \quad (7)$$

where ν is the threshold for censoring in the Gaussian process from which the Eulerian density field is generated by a lognormal transformation: $1 + \delta_{\text{LN}} = \exp(\delta_{\text{G}} - \sigma^2/2)$, where δ_{LN} and δ_{G} are the fractional overdensities in the lognormal and Gaussian field, respectively; σ^2 is the variance of the latter; and erf denotes the error function. A more meaningful way to express the threshold is in terms of the fraction, f_M , of mass below the threshold, related to the Gaussian field by

$$f_M = 0.5 \left[1 + \text{erf} \left(\frac{\nu - \sigma}{\sqrt{2}} \right) \right]. \quad (8)$$

We shall generally use f_M to define density thresholds in this paper, although, equivalently, one could use f_V , the fraction of the volume which is censored (i.e. given zero galaxy density), given by

$$f_V = 0.5 \left[1 + \text{erf} \left(\frac{\nu}{\sqrt{2}} \right) \right]. \quad (9)$$

In the case of $B = 1$ equation (7) reduces to the result derived by Catelan et al. (1994) for their weighted bias model, once account has been taken of the presence of an unwanted factor of $1/\sqrt{2}$ in the definition of their quantity $\tilde{\nu}$.

In order to compare the large-scale bias level, b_{LN} , predicted for a particular bias scheme by the lognormal model with that derived from a numerical simulation, we need to estimate σ^2 . Given that the density field is not exactly lognormal, the determination of σ^2 will not be unique. We estimate it by least-squares fitting to the differential form of (8), using (9) to relate the parameter ν to the mass density: in what follows we show that the efficacy of the lognormal model may be judged independent of any problems in estimating σ^2 .

2.3 Cen-Ostriker bias

The final model we consider is inspired by the work of CO, who found a tight $\rho_g - \rho_m$ relation well fitted by the form

$$\ln \left(\frac{\rho_g}{\tilde{\rho}_g} \right) = C_0 + C_1 \ln \left(\frac{\rho_m}{\tilde{\rho}_m} \right) + C_2 \left[\ln \left(\frac{\rho_m}{\tilde{\rho}_m} \right) \right]^2. \quad (10)$$

This is a generalisation of power law bias, with the introduction of the second parameter allowing greater freedom for the variation of the $\rho_m - \rho_g$ relationship: for example, with $C_2 < 0$ one may mitigate the effects that a large power law bias has in the densest environments. Although Cen & Ostriker found specific values for C_0 , C_1 and C_2 , we take them to be free parameters in this analysis. The value of b_{LN} for the CO models is given by

$$b_{\text{LN}} = \frac{C_1 - C_2 \sigma^2}{1 - 2C_2 \sigma^2}, \quad (11)$$

as shown in the Appendix. This model has also been studied by Little & Weinberg (1994), who investigated the void probability function under CO bias.

3 MODEL GALAXY POWER SPECTRA

For each of the models considered, we compute a galaxy power spectrum from the weighted particle distribution in a numerical simulation. The power spectrum is generally still biased on the scale of the fundamental mode, so the galaxy power spectrum is extended to larger scales by assuming a constant bias on larger scales (see Section 3.2).

3.1 Small scales: numerical simulations

Our numerical simulations were produced using the AP3M code of Couchman (1991). All simulations were of an Einstein - de Sitter universe, and used the CDM transfer function of BBKS:

$$T(k) = \frac{\ln(1 + 2.34q)}{2.34q} \times \left[1 + 3.89q + (16.1q)^2 + (5.46q)^3 + (6.71q)^4 \right]^{-1/4}, \quad (12)$$

where

$$q \equiv k/\Gamma^*, \quad (13)$$

wavenumbers, k , are in units of $h \text{ Mpc}^{-1}$, the Hubble constant is $H_0 = 100h \text{ km s}^{-1} \text{ Mpc}^{-1}$, and Γ^* is the shape parameter, which for a pure CDM universe with total and baryonic density parameters Ω_0 and Ω_B respectively, is well fit (Sugiyama 1994) by the form

$$\Gamma^* = \Omega_0 h \exp(-\Omega_B - \Omega_B/\Omega_0). \quad (14)$$

(N.B. our shape parameter, Γ^* , is defined slightly differently from the Γ parameter introduced by Efstathiou, Bond & White 1992.)

We consider Γ^* to be a free parameter, so that equations (12) and (13) describe a family of CDM-like mass power spectra, $\Delta_m^2(k) \propto k^4 T^2(k)$: we consider only models with the Harrison-Zeldovich ($n = 1$) primordial power spectrum.

The form of these equations means that a particular output from a CDM-like simulation with a given value of Γ^* may be identified with a different epoch by reinterpreting the box side:

$$L_{\text{box}}/h^{-1} \text{ Mpc} \propto 1/\Gamma^*. \quad (15)$$

Changing the assumed Γ^* in this way also alters the implied value of σ_8 , so a single simulation output gives results along a locus in (Γ^*, σ_8) space. Furthermore, different time-step outputs may be used to study different loci, so spanning the whole family of CDM-like models at the present epoch. One cannot use the earliest time-steps, which bear the traces of the initial conditions, but this powerful technique can cover the interesting part of the (Γ^*, σ_8) space of mass models. The results in this paper come principally from a simulation of a $25/\Gamma^* h^{-1} \text{ Mpc}$ box with 80^3 particles.

Biasing is implemented by weighting particles according to their local density. The local density must be calculated quite carefully to avoid discreteness problems in low-density regions. We divide the simulation box into N^3 cubic cells of side ℓ , setting the density of the particles in a cell according to the number of particles in it. If, however, there are fewer than five particles in the cell, the cell side is repeatedly doubled until at least five particles are found. Essentially the assumption in this process is that there is no structure on scales smaller than the mean *local* inter-particle separation. Inevitably there are some particles in very large void regions, and it is computationally inefficient to extend this procedure of doubling cell sizes until all of these are included in cells containing at least five particles. As implemented here, this procedure stops when ~ 1 per cent of the particles remain in cells with less than five particles: the inaccuracy in the assignment of local densities to these few particles in low density regions has no bearing on the power spectrum computed for the weighted particle distribution.

The degree of smoothing applied to the density field by this process clearly depends on the value of N . In Fig. 1 we show how the level of bias produced by a particular power law bias model from Section 4 varies with the value of N : as one would expect, the small-scale bias increases with N , (as less smoothing allows greater local densities, and, thus, higher particle weights), until it saturates at a certain value of N , where the cell size becomes smaller than the size of the most overdense virialized regions, and further reduction cannot increase the smoothed densities produced. This saturation sets in at $N \simeq 100$, and we choose for the evaluation

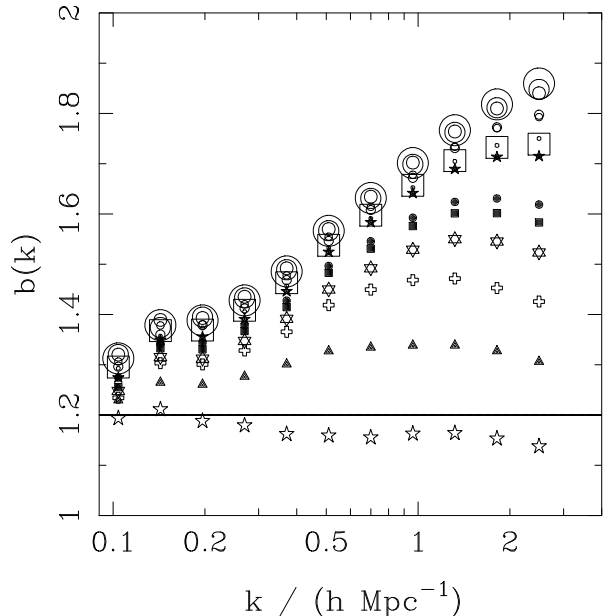


Figure 1. The scale-dependence of bias for power law bias as a function of the resolution scale used to obtain the local density: $[b(k)]^2$ is defined to be the ratio of ‘galaxy’ and mass power spectra. For a mass model with $\Gamma^* = 0.25$, $\sigma_8 = 0.64$, we apply power law biasing with $B = 1.2$. The various symbols show the results of shrinking the cell used to obtain the small-scale density contrast from $N=10$ (empty stars) to $N=140$ (largest circles). The horizontal line shows the linear bias value predicted by the lognormal model.

of our local densities a value of $N = 120$, corresponding to $\ell = 0.83(0.25/\Gamma^*) h^{-1} \text{ Mpc}$. For the mass models we are most interested in, with $\Gamma^* \simeq 0.25$, this is roughly equivalent to smoothing with a spherical top hat of filter radius $R_{\text{TH}} \simeq 0.5 h^{-1} \text{ Mpc}$, so that the scale on which we define our local density is similar to that on which cluster M/L ratios are evaluated, and on which we assume physical bias mechanisms operate. Note that, in Fig. 1 and subsequent figures, a numerical artefact means that the power in the longest-wavelength bin is slightly incorrect: the magnitude of this effect is small enough to have no bearing on our results.

3.2 Large scales: quasi-linear power spectrum extension

The range of scales which we need to consider is too large for present-day N -body simulations, so we use the method of PD94 to map linear power to non-linear power on large scales. The heart of this method, based on that of Hamilton et al. (1991) for evolving the integrated correlation function $\xi(r)$, is the pair of postulates that: (a) gravitational collapse can be considered as a translation of scales, so that wavenumbers k_L and k_{NL} in the linear and non-linear power spectrum, respectively, are related by

$$k_L = [1 + \Delta_{\text{NL}}^2(k_{\text{NL}})]^{-1/3} k_{\text{NL}}, \quad (16)$$

where $\Delta_{\text{NL}}^2(k_{\text{NL}})$ is the non-linear power spectrum; and (b) that there should be a universal mapping

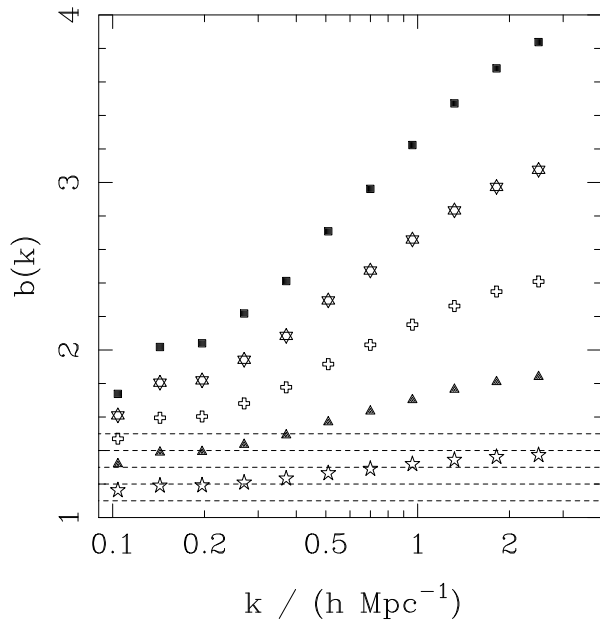


Figure 2. The scale-dependence of bias for power law bias as a function of the power law index: $B = 1.1, 1.2, 1.3, 1.4, 1.5$ in order of increasing bias. A CDM model with ($\Gamma^* = 0.25, \sigma_8 = 0.64$) is assumed. The horizontal lines show the linear bias values predicted by the lognormal model.

$\Delta_{\text{NL}}^2(k_{\text{NL}}) = f_{\text{NL}} [\Delta_{\text{L}}^2(k_{\text{L}})]$ between the linear and non-linear power spectra. PD94 used knowledge of the asymptotic behaviour of f_{NL} , together with numerical simulation data, to determine its full form. A more recent paper (Peacock & Dodds 1996) takes account of a weak dependence of f_{NL} on the linear power spectrum, but the difference between the two prescriptions is small on the quasi-linear scales in which we are interested.

To perform this extension, we take the bias parameter $b(k)$ to be constant on large scales. This is motivated by the numerical results below, which show that $b(k)$ indeed tends to a constant at small k . We estimate the constant from the smallest three wavenumber bins used in the determination of the power spectrum of the weighted particle distribution in the numerical simulation, and tests on larger boxes suggest that this procedure for estimating the asymptotic value of $b(k)$ is accurate to ~ 0.1 or better for the bias prescriptions in which we are most interested. An alternative method for setting the large-scale bias would be to use the analytic lognormal model, but, as shown in Fig. 2 and subsequent figures below, this is not usually sufficiently accurate.

4 POWER SPECTRA WITH EULERIAN BIAS

4.1 Power law bias

In Fig. 2 we show the $b(k)$ curves for a range of B values and a single mass model ($\Gamma^* = 0.25, \sigma_8 = 0.64$). As one would expect, the $b(k)$ curves steepen as B gets larger: giving more weight to over-dense regions increases the overall level of bias, as these regions are more strongly clustered than the mass distribution as a whole, but this is felt most strongly at

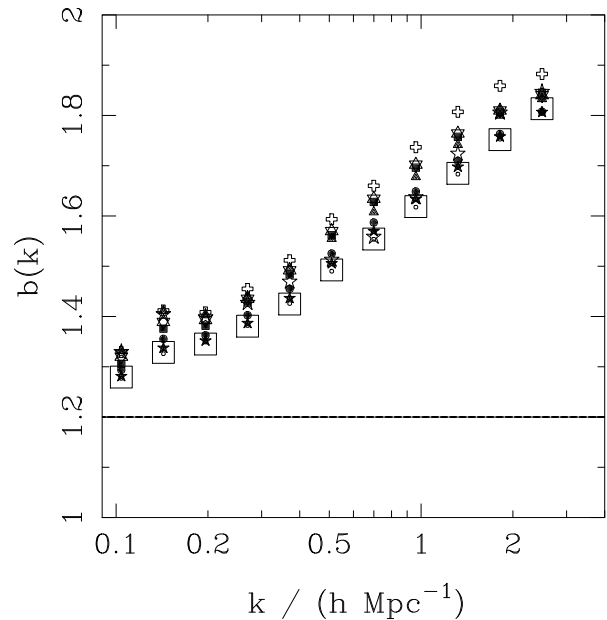


Figure 3. The scale-dependence of bias for power law bias with $B = 1.2$, for CDM models with $\Gamma^* = 0.25$ and σ_8 varying from 0.37 to 1.0. The σ_8 values plotted are as follows: 0.37 (empty stars), 0.47 (triangles), 0.56 (crosses), 0.64 (stars of David), 0.72 (filled squares), 0.80 (filled circles), 0.87 (filled stars), 0.93 (empty squares), and 1.0 (empty circles). Note that the trend of bias at given k is not monotonic with σ_8 , and that the maximum bias is attained at $\sigma_8 = 0.56$: this is discussed further in the main text. The horizontal line shows the linear bias value predicted by the lognormal model.

high k , which probes clustering power on separations within the scale of these regions themselves. The dashed lines show the corresponding values of b_{LN} , which appear to yield a slight underestimate of the asymptotic level of bias.

Figs. 3 & 4 show, respectively, the effect on $b(k)$ of varying the amplitude and shape of the linear mass power spectrum. From Fig. 3 we see that $b(k)$ is remarkably insensitive to amplitude: the small-scale bias varies by only about 15 per cent between the earliest and latest epochs, although the power in those wavenumber bins increases by more than a factor of ten in that time. Detailed inspection of Fig. 3 shows that $b(k)$ at given k initially increases with increasing σ_8 to $\sigma_8 \simeq 0.6$, after which the amplitude of the $b(k)$ curve begins to fall as σ_8 increases further. One would expect $b(k)$ to increase with σ_8 , since, as σ_8 gets larger, more mass becomes concentrated in the densest environments, which increases the level of bias on all scales, but preferentially on small scales, for the reasons given above to explain Fig. 2. To understand the reduction in $b(k)$ at large σ_8 , consider what would happen if the simulation had been left running for a long time, until $\sigma_8 \gg 1$. In the limit of a very highly evolved simulation, essentially all the mass would reside in a number of very massive clumps. Applying bias to such a mass distribution would have very little effect, so we expect $b(k) \rightarrow 1$, as $\sigma_8 \rightarrow \infty$, hence a reduction in $b(k)$ for larger σ_8 . What this tells us is that the latest epochs in the sim-

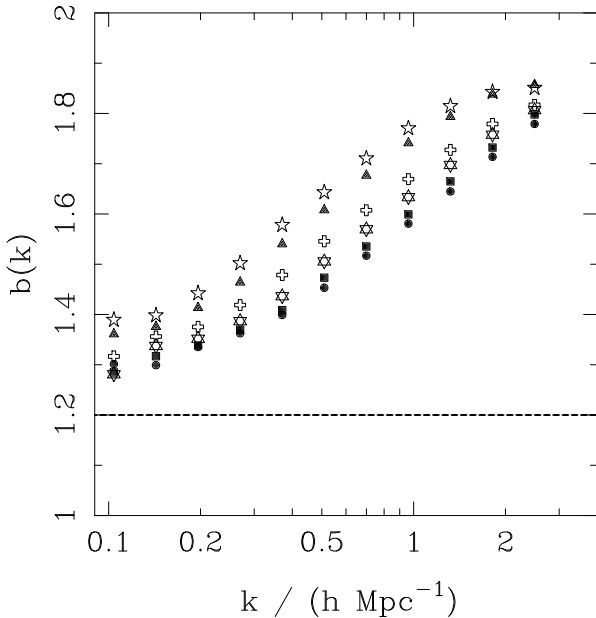


Figure 4. The scale-dependence of bias for power law bias with $B = 1.2$, for CDM models with $\sigma_8 \simeq 0.85$ and Γ^* varying from 0.175 (highest) to 0.3 (lowest). The horizontal line shows the linear bias value predicted by the lognormal model.

ulations are starting to become affected by the absence of very large-scale power beyond the box scale.

In Fig. 4 we see a slightly larger spread in $b(k)$, with models with lower Γ^* having somewhat larger bias at all wavenumbers. Given the form of the transfer function of CDM-like models (equations 12 and 13), we see that the effect of varying Γ^* at constant σ_8 can be thought of as shifting the power spectrum in wavenumber, to a model with a different degree of evolution, which is lower for the lower Γ^* values. Thus, one can imagine producing Fig. 4 by shifting the $b(k)$ curves in Fig. 3 to larger k : the value of σ_8 used for the models plotted in Fig. 4 is larger than the critical value of $\sigma_8 \simeq 0.6$, so the Fig. 3 curves one would shift would all be flattening ones in the higher σ_8 regime. In this way, we see that the variation in $b(k)$ with Γ^* shown in Fig.4 reflects how concentrated into large, discrete clumps is the mass in a CDM-like model at constant σ_8 as a function of Γ^* , which determines how large an effect is produced by biasing that mass distribution.

Overall, the main features of these plots are that the bias is a monotonic function of scale and that it varies relatively slowly as a function of scale, changing from e.g. 1.5 to 3.0 over a range of scales where the observed $\Delta^2(k)$ alters by a factor of more than 300. The slow variation of $b(k)$ is in marked contrast to the lognormal prediction: $1 + \xi_g = (1 + \xi_m)^{B^2}$, where ξ_m and ξ_g are, respectively, the mass and galaxy correlation functions. For $B = 1.5$, this implies an effective bias of 75 at $\xi = 1000$, which is a far more rapid variation than is seen in the N -body results. Note also that the lognormal model predictions indicated by the horizontal lines in Figs. 2-4 always appear to lie below the asymptotes towards which the numerical $b(k)$ curves are tending.

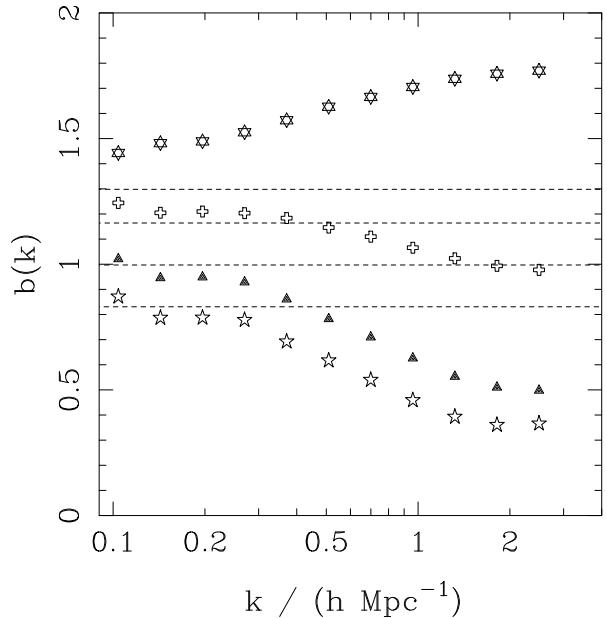


Figure 5. The scale dependence of bias for CO bias with $C_1 = 1.5$ and C_2 varying from -0.4 (lowest) to -0.05 (highest), for a mass model with $\Gamma^* = 0.25$ and $\sigma_8 = 0.64$. The horizontal line shows the linear bias value predicted by the lognormal model.

4.2 Cen-Ostriker bias

The $b(k)$ curves resulting from biasing the mass model of Fig. 1 by a series of CO models are shown in Fig. 5: the value of C_1 is held constant and C_2 is varied, to show the sensitivity of the model galaxy power spectrum to the weighting of the very densest regions. Note that, for $C_2 < 0$, the suppression of the weight given to the densest regions reduces the overall level of bias, so that the large-scale asymptote, b_∞ , falls below $b_\infty = C_1$, and that there is a change in the shape of the $b(k)$ curve, making $b(k)$ increase with scale. The lognormal predictions are shown on Fig. 5, and capture the main effect of varying C_2 : nevertheless, as with pure power law bias, the model does not predict the asymptotic level of bias perfectly.

Coles (1993) showed that local biasing of a density field which is Gaussian, or a local transformation thereof, will produce a real-space bias parameter, $b(r)$, (defined to be the square root of the ratio of the galaxy and mass correlation functions) which decreases monotonically with scale. For CDM-like spectra, the same analysis predicts a monotonic decrease in $b(k)$ with increasing scale, with the exception of the very largest scales ($k \lesssim 0.01 h \text{ Mpc}^{-1}$), where the tangent spectral index is $n_{\text{eff}} > 0$ and, consequently, $b(k)$ can increase unboundedly. The results of Fig. 5 show how the Coles (1993) inequalities breaks down once the mass distribution becomes sufficiently non-linear; like the failure of the lognormal model to predict correctly the large-scale asymptotic bias level, this indicates that the evolved mass distribution is not well described by a lognormal.

4.3 Censoring

The result of censoring the same mass model is shown in Fig. 6, which indicates that the level of bias increases as more of the void regions are removed. However, it is only when $f_M \gtrsim 0.6$ that the curvature in $b(k)$ begins to increase appreciably, showing again how the small-scale power is determined by the densest regions of space. The same can be said for Fig. 7, which shows the same effect in the censoring of a $B = 1.2$ power law bias model at various thresholds. The dashed lines are the predictions of the lognormal model, which once again produces a fair, but not perfect, estimate of the level of large-scale bias.

Both in the lognormal approximation, and in the numerical datasets, the effects of censoring seem less extreme than might have been expected on the basis of the following naive argument. If we make up the mass distribution by the addition of an unclustered background to a clustered field, then censoring might be expected to correspond roughly to the removal of the unclustered part. If we write

$$\bar{\rho}(1 + \delta) = \bar{\rho}_c(1 + \delta_c) + \rho_u, \quad (17)$$

then we have

$$\delta_c = [1 + \rho_u/\bar{\rho}_c] \delta, \quad (18)$$

so that the effective real-space bias is just $b = (1 - f_M)^{-1}$, where $f_M = \rho_u/(\bar{\rho}_c + \rho_u)$ is the fraction of the mass which has been censored. To solve the M/L problem by censoring alone, we would need $f_M \simeq 0.8$, implying $b = 5$ by this argument. However, the lognormal model yields only $b = 1.56$ for $f_M = 0.8$ (assuming $\sigma = 2.5$, but only weakly dependent on σ): so, an amount of censoring large enough to have an important effect on M/L values thus produces the sort of bias factor needed in reality to give a sensible σ_8 if $\Omega = 1$.

4.4 Scale dependence of bias

One interesting general feature of the bias seen in the numerical results is the relatively weak scale dependence. Consider the prediction in case of power law bias of a lognormal field, as given in the Appendix:

$$1 + \xi_g = (1 + \xi_m)^{B^2}. \quad (19)$$

This implies a very rapid increase of bias, once the field reaches scales where the fluctuations are non-linear.

Even for the case of power law bias, such a rapid dependence on scale is not seen in our N -body data, as illustrated for a variety of models below in Fig. 8. This plot shows a fitting formula for the scale-dependence of bias in k space, which is inspired by the lognormal form, but which introduces an extra parameter in order to allow pure scale-independent bias as one limit:

$$1 + \Delta_g^2 = (1 + b_1 \Delta_m^2)^{b_2}. \quad (20)$$

As may be seen from the figure, this form is capable of giving an excellent description of the data. For pure power law bias, the results scale with B almost exactly as

$$(b_1, b_2) = (B^{1.8}, B^{0.7}), \quad (21)$$

so the non-linear component of the bias is much smaller than the scale-independent component: this is a general feature of all the models we have investigated.

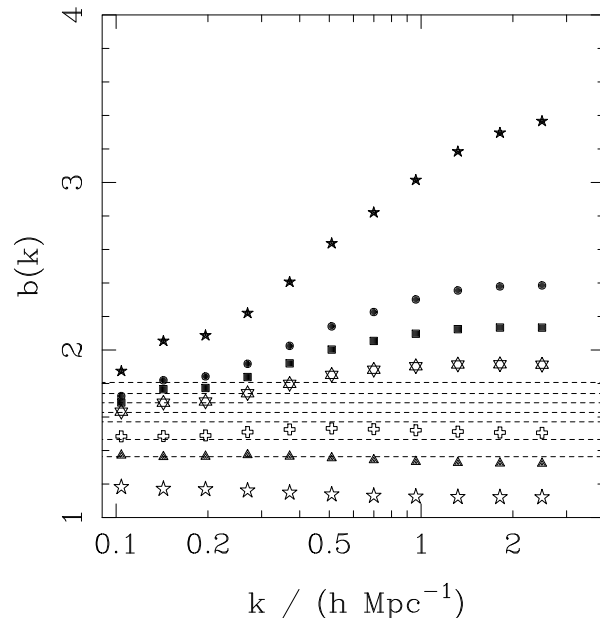


Figure 6. The scale-dependence of bias for censoring bias with f_M varying from 0.35 (lowest) to 0.65 (highest), for a mass model with $\Gamma^* = 0.25$ and $\sigma_8 = 0.64$. The horizontal lines show the linear bias values predicted by the lognormal model.

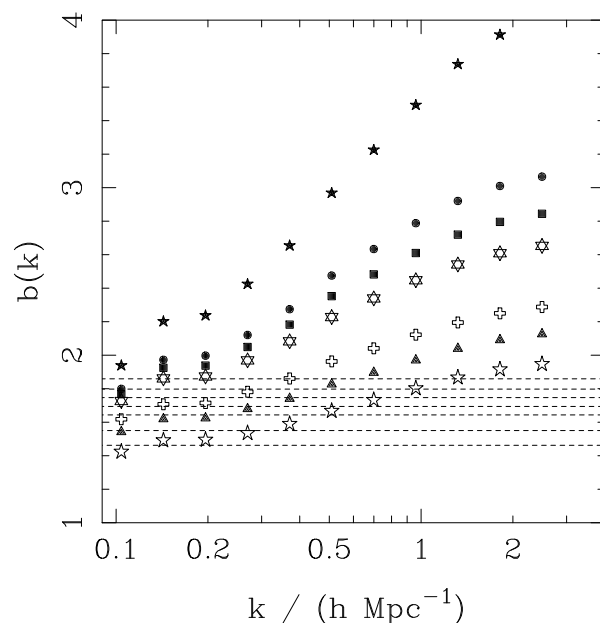


Figure 7. The scale dependence of bias for a combination of power law bias with $B = 1.2$ and censoring with f_M varying from 0.35 (lowest) to 0.65 (highest), for a mass model with $\Gamma^* = 0.25$ and $\sigma_8 = 0.64$. The horizontal lines show the linear bias values predicted by the lognormal model.

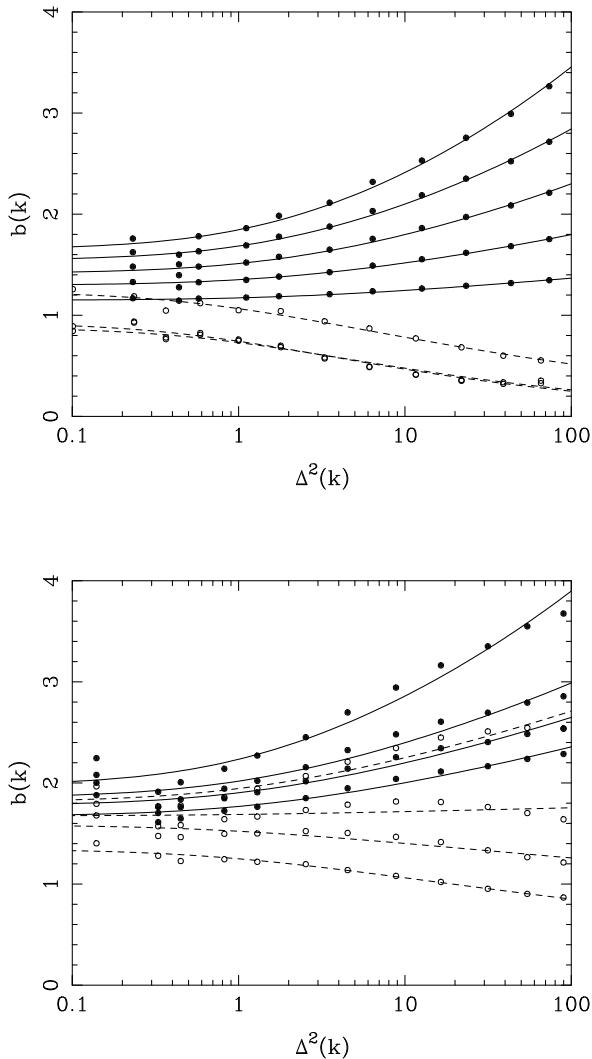


Figure 8. Numerical data for $b(k)$ and model fits. This figure considers the case $\Gamma^* = 0.25, \sigma_8 = 1$ only. The top panel shows pure power law bias with $B = 1.1, 1.2, 1.3, 1.4, 1.5$ (solid points and full lines) and CO bias with $C_1 = 1.2$ and $C_2 = -0.1, -0.4, -0.7$ (open points and dashed lines). The bottom panel shows a combination of censoring ($f_M = 0.3, 0.4, 0.5, 0.6$) with power law bias: $B = 0.8$ (solid points and full lines) and $B = 1.2$ (open points and dashed lines).

Notice also that the power law models have a large-scale linear bias of $b_\infty = [b_1 b_2]^{1/2} \simeq B^{1.3}$, which is larger than the simple relation $b_\infty = B$ expected from the lognormal model. The lognormal model therefore fails quite badly as a model for the non-linear density field produced in strong gravitational non-linear evolution, which should come as no surprise: the models studied in the Appendix are invaluable as heuristic aids, but should not be applied quantitatively to the real Universe.

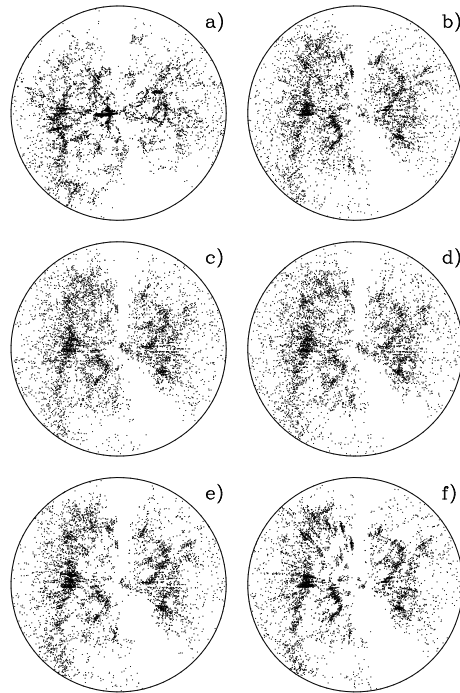


Figure 9. A plot of the CfA slice [$30^\circ < \delta < 60^\circ$; $V < 12000 \text{ km s}^{-1}$] (panel a), with a variety of synthetic N -body simulations having the same selection function and numbers of ‘galaxies’. The simulations used $n = -1.5$ initial conditions, with $\Omega = 0.3$ in panel (b) and $\Omega = 1$ in panel (c). The normalization was set at $\sigma_8 = 1.0$ in (b) and 0.6 in (c). Panels (d) and (e) bias the $\Omega = 1$ data with respectively $B = 1.23$ and $B = 1.23, f_M = 0.1$. Panel (f) biases the open simulation with $f_M = 0.1$. It appears that censoring is needed in both cases to obtain sufficiently empty voids.

5 COMPARISON OF CDM-LIKE MODELS WITH OBSERVED GALAXY CLUSTERING

We now attempt to use some of the above results to investigate which models are capable of accounting for the observed statistics of galaxy clustering. This can be approached at a number of levels, of which the simplest is the study of the fluctuation spectrum. We shall mainly restrict ourselves to this question here, but it may be useful to begin by illustrating in more detail the effect of our bias models on the simulated galaxy density field.

Fig. 9 compares the true local galaxy distribution with various models. In panel (a) we show the local ($V < 1200 \text{ km s}^{-1}$) distribution of galaxies from the CfA slice (Huchra et al. 1992, with more recent updates), while simulations (b) and (c) show unbiased $\Omega = 0.3$ and $\Omega = 1$ universes, respectively, for a mass model whose linear power spectrum has a slope ($n = -1.5$) roughly equaling that of CDM on galactic scales and a normalization set by the cluster abundances. The clearest feature of these examples is an

insufficient contrast between high density regions and voids. Panel (d) applies power law bias with $B = 1.23$ to the $\Omega = 1$ case, but this improves the situation only slightly. Panel (e) adds censoring with $f_M = 0.1$, and this ‘opens out’ the voids to roughly the correct extent. Finally, panel (f) applies the same censoring to the low density model, again with reasonable results at the visual level. We thus believe that our bias models do capture the main essentials of the modifications needed in order to make dark matter distributions resemble the real distribution of galaxies. For the remainder of the present paper, we shall be content to restrict ourselves to comparison of data and model at the two-point level.

5.1 Observational data

The observational data we use for comparison with the models are:

(i) Large-scale normalisation: the four-year *COBE* data yield $Q_{\text{rms-PS}} = 18.4 \mu\text{K}$ (e.g. Tegmark 1997). We allow a conservative 10 per cent uncertainty in that figure.

(ii) Intermediate scale normalisation: $\sigma_8 = 0.57 \pm 0.05$ from the abundance of rich clusters (White et al. 1993). We consider models with $0.5 < \sigma_8 < 0.7$.

(iii) Galaxy clustering: real-space APM galaxy power spectrum (Baugh & Efstathiou 1993) over the wavenumber range $-1.5 \leq \log_{10}(k/h \text{Mpc}^{-1}) \leq 0.5$.

The galaxy clustering range chosen spans the apparent point of inflection in the APM power spectrum, including data on the linear scales studied by PD94, as well as the non-linear regime omitted from their analysis. We have not used the largest scales because of possible uncertainties in surface uniformity of the survey, and have multiplied the power spectrum of Baugh & Efstathiou (1993) by 1.25 to account for the non-zero median redshift of the APM survey: see Peacock (1997) for details of that correction.

For models which satisfy the above constraints, we investigate whether they can give sufficiently large mass-to-light ratios in clusters. In rough terms, we require $\rho_g/\bar{\rho}_g \simeq 5000$ in regions where $\rho_m/\bar{\rho}_m \simeq 1000$. One can argue in detail about these numbers, but they should be approximately correct for cluster masses and sizes: in fact, as we shall see, no model gets close to the required galaxy density.

We note in passing that we find that no Γ^* model can be linearly biased [i.e. $\Delta_g^2 = b^2(k)\Delta_m^2$, with $b(k)$ constant] in such a way as to satisfy these three constraints. The problem lies with the shapes of the evolved mass power spectra of CDM-like models, which do not match that of the APM power spectrum, implying that to bias successfully a Γ^* model will require a non-linear $b(k)$, and thus motivating our study of non-linear bias prescriptions. In any case, it is not clear how a linear bias may be achieved from a local transformation of a highly non-linear density field, although numerical studies involving detailed prescriptions for galaxy formation have shown a nearly linear bias (Kauffmann, Nusser & Steinmetz 1997).

5.2 Results

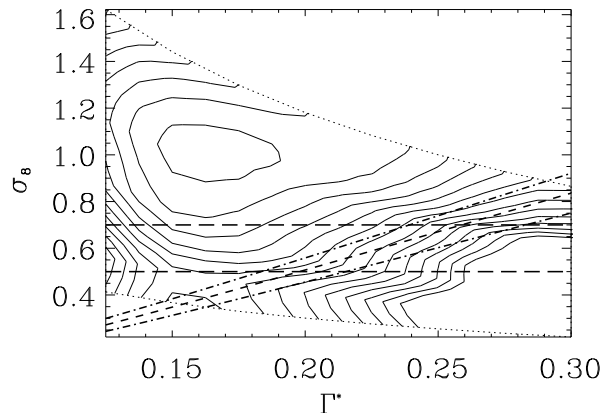


Figure 10. Contours of χ^2 between power law biased CDM power spectra and the APM data: the contours are at $\Delta\chi^2 = 15$, with $\chi^2 = 30$ being the lowest contour shown, near the minimum at $\Gamma^* \simeq 0.17$, $\sigma_8 \simeq 1.0$. The horizontal lines show the allowed range of σ_8 from the cluster abundance constraint. The diagonal lines show the constraint required to satisfy the *COBE* measurement for the case of no tilt.

5.2.1 Power law bias

In Fig. 10 we show contours of χ^2 for fits of power law biased CDM-like models to the APM data. There is a clear preferred model, with $\Gamma^* = 0.175$, $\sigma_8 = 1.03$, $B = 0.86$ and $\chi^2 = 14.5$, for 13 degrees of freedom: the power spectra are compared at 14 wavenumbers, so there are 13 degrees of freedom in the power law bias fits and 12 in the (B, f_M) and (C_1, C_2) fits. This model is however firmly excluded both by the cluster abundance constraint (horizontal lines) and *COBE* (angled lines) if the primordial spectral index is $n = 1$. This latter constraint is removed if the spectrum is tilted, but even so the cluster abundance difficulty remains. If we insist on a normalization of $\sigma_8 \simeq 0.6$, to fit the cluster abundance normalisation, the preferred value of Γ^* is unchanged at 0.175, B increases to 1.1 and χ^2 increases sharply to 43.3. These models are compared to the APM data in Fig. 11. Neither alternative fully reproduces the observed data, especially those below the inflection around $k \simeq 0.1 h \text{Mpc}^{-1}$, but they exploit the errors in order to reduce the discrepancy to the point where the overall χ^2 is moderate.

The best-fitting values of B for the models of Fig. 10 are plotted in Fig. 12. The contour lines (for $B \gtrsim 0.8$) are very close to being lines of constant σ_8 . Since σ_8 is related roughly to a scale $k \sim 0.3 h \text{Mpc}^{-1}$, which is close to the asymptotic region where $b(k)$ is constant, this indicates that the most important effect of the bias is in setting the normalisation, rather than the detailed shape, of the galaxy power spectrum: this bears out the results given in equation (21). Note that Fig. 10 shows that χ^2 decreases slightly as σ_8 falls below 0.4 for $\Gamma^* = 0.15 - 0.20$, and, from Fig. 12, the best fit B values $B \sim 1.5$ are much higher than those near the global χ^2 minimum. This indicates how, given the linear power spectrum of a particular mass model, there are two ways to try to achieve the steepening required to match the APM power spectrum: use a high bias on a moderately

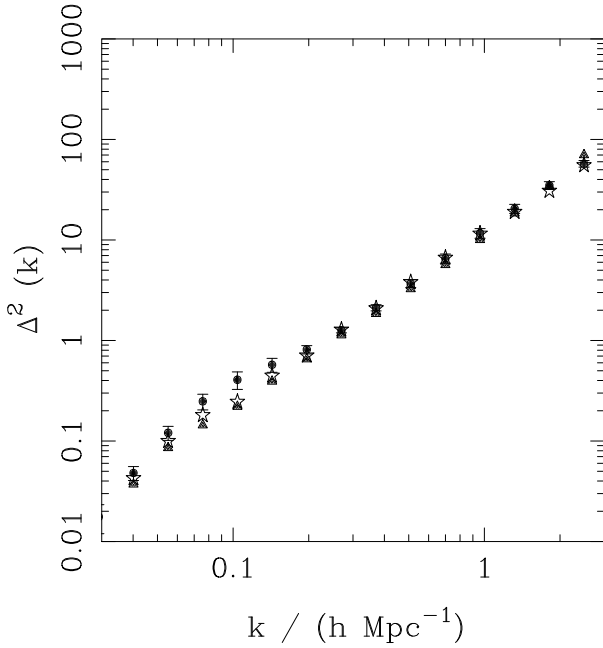


Figure 11. A comparison between the APM data (filled circles) and two power law biased CDM models: the stars show $\Gamma^* \simeq 0.17$, $\sigma_8 = 1.0$, $B = 0.85$, and the triangles show $\Gamma^* \simeq 0.17$, $\sigma_8 = 0.55$, $B = 1.3$.

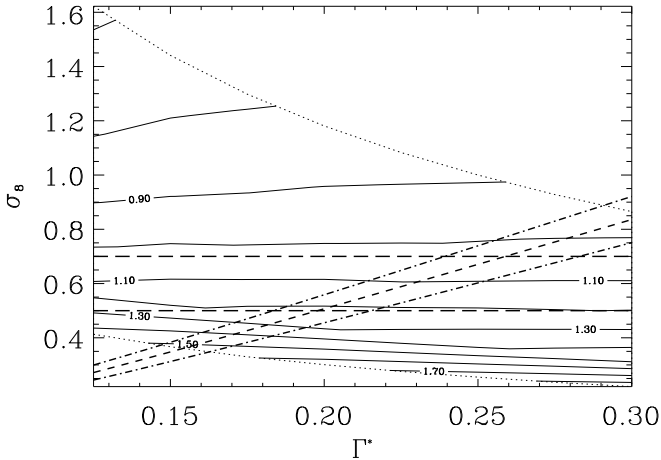


Figure 12. The best-fitting value of B in power law bias models, as a function of (Γ^*, σ_8) . The horizontal lines show the allowed range of σ_8 from the cluster abundance constraint. The diagonal lines show the constraint required to satisfy the *COBE* measurement for the case of no tilt.

evolved mass distribution, or evolve the mass distribution much more and use anti-bias ($B < 1$) to pull down the power to the desired level.

5.2.2 Cen-Ostriker bias

For the remainder of our analysis we restrict our attention to the region of the (Γ^*, σ_8) plane which satisfies both our normalisation criteria. The form of the $\chi^2(C_1, C_2)$ surface

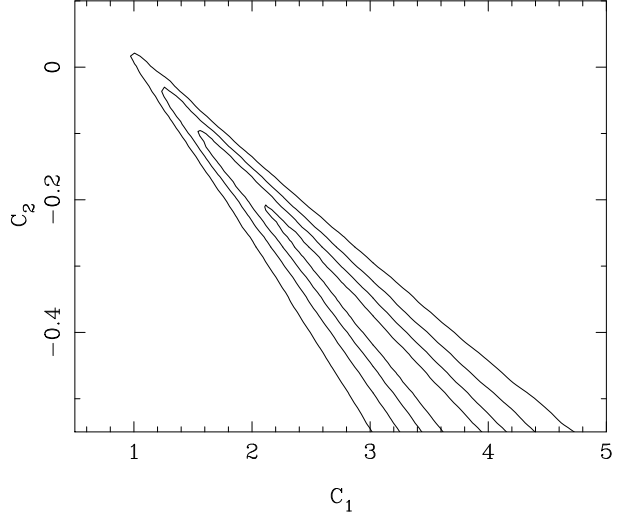


Figure 13. Contours of χ^2 as a function of the CO parameters C_1 & C_2 in the comparison between biased CDM power spectra and the APM data. The contours are at $\Delta(\log_{10} \chi^2) = 0.3$ above $\chi^2 = 1$.

for these mass models has a very characteristic form, as illustrated by Fig. 13, which shows it for one such model, with ($\Gamma^* = 0.25$ and $\sigma_8 = 0.64$). In all cases the χ^2 contours form a wedge-shaped valley in the (C_1, C_2) plane, the gross features of which are readily explained. The introduction of the C_2 term into the bias formula allows these mass models to improve agreement with the APM power spectrum by maintaining their large-scale power (by increasing C_1 above the value of the best-fit B value) in the face of its suppression by the negative C_2 value which is needed so as not to produce too much small-scale power. The floor of the valley in the χ^2 surface gently rises with increasing C_1 , but we need not concern ourselves with whether or not models matching the APM power spectrum are to be found at large C_1 , since the increasingly negative value of C_2 required to make that match very rapidly reduces the predicted cluster M/L ratio to very low values. In fact, acceptable χ^2 values are rarely found above $C_1 = 2$, and the negative C_2 values required by acceptable models means that their mass-to-light ratios fall short by factors of several hundred from that required to reconcile observed cluster M/L values with $\Omega = 1$. We therefore exclude all CDM-like models biased according to the Cen-Ostriker formula.

5.2.3 Censored models

In Fig. 14 we plot $\chi^2(B, f_M)$ for a particular allowed mass model ($\Gamma^* = 0.25, \sigma_8 = 0.64$ again). The basic form of this curve is, again, characteristic and easy to understand: as more and more weakly-clustered mass is censored, a lower value of B is required to match the APM power spectrum to a given accuracy. Typically, the best-fit censored power law model has $f_M \simeq 0.35 - 0.45$ and a value of B lower than that for the best pure power law bias model. Those censored power law bias models that give a good fit to the APM power

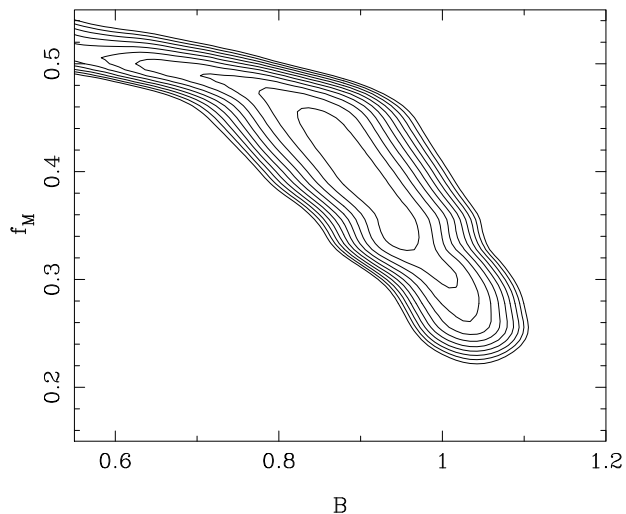


Figure 14. Contours of χ^2 for the bias model with power law bias and censoring, as a function of the parameters B and f_M , in the comparison between biased CDM power spectra and the APM data. The contours are $\Delta\chi^2 = 15$, with the inner contour being $\chi^2 = 30$.

spectrum may be excluded on M/L ratio grounds, as is clear from Fig. 14, which shows that increasing f_M only leads to lower values of B : e.g. censoring half the mass increases the mass-to-light ratio by a factor of two, but the low value of B reduces it by a very much larger factor.

5.3 Comparison of bias prescriptions

An enlightening comparison of the effects of the three bias prescriptions is provided by Figs. 15 and 16. In Fig. 15, the filled circles show the APM galaxy power spectrum, while the stars of David show the mass power spectrum for a model with $\Gamma^* = 0.25$ and $\sigma_8 = 0.64$. Clearly, to match the APM power spectrum, this mass model needs a significant bias on large scales, below the inflection in the APM power spectrum. However, the required level of bias falls with increasing wavenumber, and there is little room for bias on the smallest scales. The best fit power law bias model yields $\chi^2 = 96.2$ at $B = 1.07$, and its power spectrum is shown by the stars in Fig. 15, where it is clear that only a modest power law bias produces too much small-scale power, while falling short of the desired clustering strength on large scales. The freedom to censor mass produces the power spectrum given by the triangles in Fig. 15, which has $B = 0.93$ and $f_M = 0.38$ (giving $\chi^2 = 62.3$), while the best fit Cen-Ostriker model is $C_1 = 2.0$, $C_2 = -0.19$, (crosses), which yields $\chi^2 = 27.1$. The different effects of these three models are better shown by their $b(k)$ curves, which are plotted in Fig. 16. Censoring almost 40 per cent of the mass produces the required increase in large-scale power, but $B < 1$ is required to restrict the level of small-scale clustering, which still exceeds that of APM galaxies. The great freedom afforded by the introduction of the C_2 parameter is shown by the much larger χ^2 reduction it allows, as well as by the shape of the $b(k)$ curve

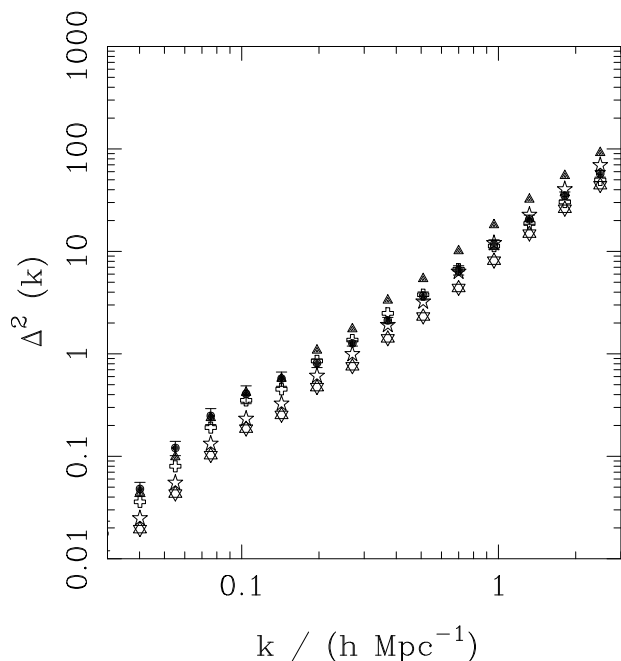


Figure 15. Biasing a mass model to fit the APM power spectrum. The mass power spectrum for a model with $\Gamma^* = 0.25$ and $\sigma_8 = 0.64$ is shown by the stars of David, while the filled circles plot the APM power spectrum. The best fit models from the three bias prescriptions are shown as follows: (a) power law bias with $B = 1.07$ (stars); (b) censored power law bias with $B = 0.93$ and $f_M = 0.38$ (triangles); and (c) Cen-Ostriker bias with $C_1 = 2.0$ and $C_2 = -0.19$ (crosses).

it produces in Fig. 16: a much better fit to the APM power spectrum is obtained, as equation (10) allows a substantial large-scale bias at the same time as keeping the small-scale clustering power pinned, rising only slightly above the level of that found in the mass distribution. The problem with this model, of course, is that it fails to provide a sufficiently large boost to M/L on scales of clusters. There appears to be no way in which we can achieve the necessary $b(k)$ without violating this constraint.

6 DISCUSSION AND CONCLUSIONS

We have investigated the effect of local biasing on the clustering statistics of galaxies. In general, we find that local biasing gives rise to a scale-dependent bias, so the shape of galaxy power spectrum no longer directly reflects the underlying mass distribution. However, the change in $b(k)$ with scale is often rather modest: if $b_\infty \simeq 1.5$, as suggested by observations and *COBE* normalisation, then the models we have investigated would only predict at most $b(k) \simeq 3$ at $k \simeq 1 \text{ h Mpc}^{-1}$. The scale dependence of the bias appears to be monotonic, but $b(k)$ does not decrease with scale in all cases, showing how the inequalities of Coles (1993) break down once the density field is sufficiently non-linear that it is no longer well described by a Gaussian field, or a local transformation thereof. The $b(k)$ curves produced by our biasing prescriptions are also quite smooth, so it would appear that any model capable of producing sharp changes in

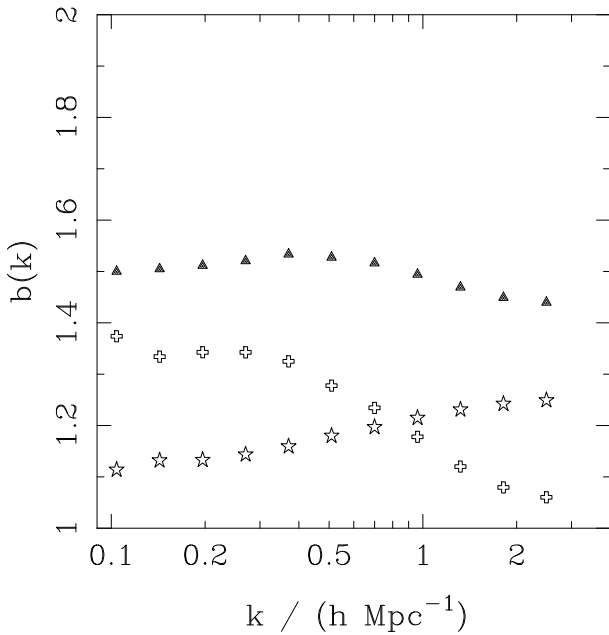


Figure 16. The scale dependence of the bias in the three galaxy power spectra shown in Fig. 15: (a) power law bias with $B = 1.07$ (stars); (b) censored power law bias with $B = 0.93$ and $f_M = 0.38$ (triangles); and (c) Cen-Ostriker bias with $C_1 = 2.0$ and $C_2 = -0.19$ (crosses).

galaxy power with respect to that of the mass would have to involve non-local bias.

The scale dependence of bias clearly presents difficulties in the interpretation of observed galaxy clustering, by allowing a wider range of mass power spectra to map onto the galaxy power spectrum data through the use of a suitably curved $b(k)$. Interpretation of even these models is simplified on large scales, however, where the bias tends to a constant value.

We have looked at a range of galaxy clustering models in the context of an Einstein - de Sitter universe, to see if any of these models can simultaneously fit the APM power spectrum and the observed mass-to-light ratios in clusters of galaxies. The strong conclusion we reach is that *COBE*-normalised CDM-like models with σ_8 fixed as required by the observed abundances of clusters do not succeed, given the biasing functions we have explored. In addition, the models fail to reproduce the required mass-to-light ratios by large factors, so if any successful bias function were found, it would probably be rather pathological.

There are several ways to improve the agreement of the models with observation. One is to lower the density below $\Omega = 1$, thus reducing or removing the constraints on our models in the high-density regions. The lower Ω has the effect of increasing the required σ_8 from cluster abundances, but the non-linear effects on the mass spectrum depend on Ω only on scales smaller than those we have considered here (Peacock & Dodds 1996). The second is to change the shape of the underlying power spectrum to one with a sharper break than CDM, such as mixed dark matter (e.g. Taylor & Rowan-Robinson 1992; van Dalen & Schaeffer 1992; Klypin et al. 1993). This latter possibility is the only existing model

which can explain the full inflection in the APM power spectrum around $k \simeq 0.1 h \text{ Mpc}^{-1}$, since CDM-like models produce a much smoother variation at this point.

The conclusions we draw from our results are thus as follows:

- (i) No linearly-biased CDM-like model can reproduce the APM power spectrum: a non-linear $b(k)$ curve is required if the cosmological fluctuations spectrum is one of the Γ^* models given by equations (12) and (13). Analyses (such as that of PD94) which do allow a linearly-biased Γ^* model can do so only because they ignore clustering data on non-linear scales, which greatly weakens their power to reject models.
- (ii) Non-linear bias prescriptions generically produce a scale-dependent bias, but it is difficult to produce a strongly curved $b(k)$ relation with Eulerian bias, so a confirmation of the APM inflection would be strong evidence for some feature in the primordial linear spectrum at that scale or for non-local bias in galaxy clustering.
- (iii) Analytical models based on a lognormal mass distribution are useful heuristics for gauging the rough level of the large-scale bias produced by a given prescription, but they are not sufficiently accurate to replace numerical simulations.
- (iv) No Einstein - de Sitter CDM-like mass model can be biased, using the range of bias prescriptions studied here, to match the APM power spectrum if it is required to be *COBE*-normalised and account for the abundances and M/L values of clusters of galaxies: if these conditions are to be satisfied using the bias models considered here, then the mass power spectrum must be flatter than CDM-like models on small scales.

ACKNOWLEDGEMENTS

RGM acknowledges support from PPARC rolling grants at QMW and Imperial College. We thank Ed Bertschinger and Jim Gelb for numerical simulation data used at an early stage of this project, John Huchra for the use of the ZCAT redshift compilation and an anonymous referee for comments that clarified the presentation of several points in this paper.

REFERENCES

- Babul A., White S.D.M., 1991, MNRAS, 253, 31P
 Bardeen J.M., Bond J.R., Kaiser N., Szalay A.S., 1986, ApJ, 304, 15 (BBKS)
 Baugh C.M., Efstathiou G., 1993, MNRAS, 265, 145
 Catelan P., Coles P., Matarrese S., Moscardini L., 1994, MNRAS, 268, 966
 Cen R.Y., Ostriker J.P., 1992, ApJ, 399, L13 (CO)
 Cole S., Kaiser N., 1989, MNRAS, 237, 1127
 Coles P., 1993, MNRAS, 262, 1065
 Coles P., Jones B., 1991, MNRAS, 248, 1
 Couchman H.M.P., 1991, ApJ, 368, L23
 Davis M., Efstathiou G., Frenk C.S., White S.D.M., 1985, ApJ, 292, 371
 Dekel A., Rees M.J., 1987, Nat, 326, 455

- Efstathiou G., Bond J.R., White S.D.M., 1992, MNRAS, 258, 1P
- Hamilton A.J.S., Kumar P., Lu E., Matthews A., 1991, ApJ, 374, L1
- Huchra J., Geller M., Clemens C., Tokarz S., Michel A., 1992, Bull. C.D.S. 41, 31
- Kaiser N., 1984, ApJ, 284, L9
- Kauffmann G., Nusser A., Steinmetz M., 1997, MNRAS, 286, 795
- Katz N., Quinn T., Gelb J.M., 1993, MNRAS, 265, 689
- Klypin A., Holtzman J., Primack J., Regős E., 1993, ApJ, 416, 1
- Little B., Weinberg D.H., 1994, MNRAS, 267, 605
- Mann R.G., Heavens A.F., Peacock J.A., 1993, MNRAS, 263, 798
- Matarrese S., Coles P., Lucchin F., Moscardini L., 1997, MNRAS, 286, 115
- Matarrese S., Verde L., Heavens A.F., 1997, MNRAS, in press (astro-ph/9706059)
- Mo H.J., Jing Y.P., White S.D.M., 1996, MNRAS, 282, 1096
- Mo H.J., White S.D.M., 1996, MNRAS, 282, 347
- Peacock J.A., 1997, MNRAS, 284, 885
- Peacock J.A., Dodds S.J., 1994, MNRAS, 267, 1020 (PD94)
- Peacock J.A., Dodds S.J., 1996, MNRAS, 280, L19
- Sugiyama N., 1995, ApJS, 100, 281
- Taylor A.N., Rowan-Robinson M., 1992, Nat, 359, 396
- Tegmark M., 1997, ApJ, 464 L35
- van Dalen A., Schaefer R.K., 1992, ApJ, 398, 33
- White S.D.M., Efstathiou G., Frenk C.S., 1993, MNRAS, 262, 1023

APPENDIX A: BIASED LOGNORMAL DENSITY FIELDS

The lognormal density field is a convenient analytical model in which the effects of various simple Eulerian density transformations can be calculated quite simply. The non-linear lognormal density field is produced by taking the exponential of a Gaussian density field:

$$1 + \delta_{\text{LN}} = \exp(\delta_{\text{G}} - \sigma^2/2). \quad (\text{A1})$$

The variance of the Gaussian field is σ^2 and the second term in the exponential is a normalising factor, so that $\langle \delta_{\text{LN}} \rangle = 0$. Although this transformation resembles a form of bias, and has been discussed in that context, it is important to be clear that this is not what is envisaged here. The lognormal field is a model for the mass density field: it is the simplest extension of the Gaussian random field which is physical in the sense of forbidding negative densities. The lognormal field differs from its generating Gaussian only when σ is significantly larger than zero, so the lognormal transformation should be thought of as a means of simulating the effects of non-linear gravitational instability.

A1 Power law bias

The simplest modification of a density field is a power law $\rho \propto \rho_{\text{LN}}^B \propto \exp(B\delta_{\text{G}})$.

The effects of this modification are easily deduced, since Coles & Jones (1991) showed that

$$1 + \xi_{\text{LN}} = \exp(\xi_{\text{G}}). \quad (\text{A3})$$

The power law model is just the original lognormal model with the generating Gaussian scaled by a factor B , and so

$$1 + \xi_{\text{PLN}} = \exp(B^2\xi_{\text{G}}) = (1 + \xi_{\text{LN}})^{B^2}. \quad (\text{A4})$$

Interestingly, this modification does not increase the skewness of the density field. We define the skewness parameter (not the skewness itself) as

$$S \equiv \frac{\langle \delta^3 \rangle}{(\langle \delta^2 \rangle)^2}. \quad (\text{A5})$$

Integrating over the Gaussian field gives

$$S = 2 + e^{B^2\sigma^2}. \quad (\text{A6})$$

Since the observed density rms in the linear regime is just $B\sigma$, this says that the observed skewness-variance relation is unaltered by bias, which masquerades as extra non-linearity in the mass field. This degeneracy between bias and evolution is a feature of the lognormal model. Genuine gravitational evolution leads to different shaped structures (flattened on first collapse), and bias and evolution can be separated by studying shape-dependent statistics such as the bispectrum or 3-point correlation function (e.g. Matarrese, Verde & Heavens 1997).

A2 Censoring bias

A power law provides a significant boost in density at large over-densities, but it is also plausible that the galaxy density may suffer abrupt truncation at small over-densities, i.e. in the voids.

In the case of no other bias, this is the model studied by Catelan et al. (1994). The method of evaluation is the same in all such cases: write $\delta' = f(\delta)$, where it is assumed that the function f is normalised to force $\langle \delta' \rangle = 0$, and use

$$1 + \xi' = \langle (1 + \delta'_1)(1 + \delta'_2) \rangle. \quad (\text{A7})$$

The correlation function is then

$$1 + \xi' = \int_{-\infty}^{\infty} \int_{-\infty}^{\infty} (1 + f_1)(1 + f_2) P(\delta_1, \delta_2) d\delta_1 d\delta_2, \quad (\text{A8})$$

where the Gaussian joint distribution involves the correlation coefficient $r \equiv \xi/\sigma^2$. For the case of truncated power law bias, the modified density field is

$$1 + \delta' = \frac{\exp[B\delta_{\text{G}} - B^2\sigma^2/2]}{0.5 \left[1 - \operatorname{erf}\left(\frac{\nu - B\sigma}{\sqrt{2}}\right) \right]}, \quad (\text{A9})$$

where the threshold is specified in terms of its value in the Gaussian field that generates the mass: $\delta' = -1$ for $\delta_{\text{G}} < \nu\sigma$.

For the case of censored power law bias, the correlation function reduces to the 1D integral

$$1 + \xi' = \sqrt{2/\pi} \frac{e^{-B^2\sigma^2(1+r^2)/2}}{[1 - \operatorname{erf}(\nu - B\sigma)/\sqrt{2}]^2} \times \int_{\nu}^{\infty} e^{xB\sigma(1+r) - x^2/2} \left[1 - \operatorname{erf}\left(\frac{\nu - B\sigma + r^2 B\sigma - rx}{\sqrt{2(1-r^2)}}\right) \right] dx. \quad (\text{A10})$$

In the $\xi \ll 1$ regime, this reduces to $\xi' = b_{\text{LN}}^2 r \sigma^2$, with the linear bias parameter

$$b_{\text{LN}} = B + \frac{\sqrt{2/\pi} e^{-(\nu-B\sigma)^2/2}}{\sigma \left[1 - \text{erf} \left(\frac{\nu-B\sigma}{\sqrt{2}} \right) \right]}. \quad (\text{A11})$$

which reduces to the result of Catelan et al. (1994) for $B = 1$, once allowance is made for a spurious factor of $1/\sqrt{2}$ in their equation (19).

The results for the case of censoring (with or without power law bias) are hardly transparent, and it may be helpful to illustrate them in one particular case. Consider the following model for the galaxy correlation function, shown in Fig. A1:

$$\xi = [\xi_{\text{max}}^{-1} + (r/r_0)^\gamma]^{-1}. \quad (\text{A12})$$

For the case of pure power law bias, it is simple to recover the corresponding mass correlation function, and to obtain from this the correlation function for the Gaussian process which would generate the mass field as a lognormal process. We shall consider the specific case $B = 1.23$. We also take $\xi_{\text{max}} = 10^4$, giving $\sigma = 2.47$, although this is not critical.

We now compare the action of censoring bias on the same mass field. To achieve the same linear bias of 1.23 requires a threshold $\nu = 2.1$, corresponding to censoring 98 per cent of the volume and 36 per cent of the mass. As a perhaps more realistic compromise model, we consider censoring and power law bias in combination. A threshold of $\nu = 1.3$ censors 90 per cent of the volume and 12 per cent of the mass, and requires $B = 1.18$ for the same linear bias. These alternatives are compared in Figure A1. We see that censoring alone steepens the correlation function, but not to the same extent as power law bias with the same large-scale bias. An excellent fit (not shown, as it is hard to see any deviation) is obtained with the two parameter formula

$$1 + \xi' = (1 + b_1 \xi)^{b_2}, \quad (\text{A13})$$

which is of course a perfect fit in the power law only case. For censoring only, $(b_1, b_2) = (1.35, 1.12)$ is needed, changing to $(1.09, 1.39)$ in the combination case.

Although this is only one example, the general behaviour follows this trend: for a given linear bias, censoring is less effective at steepening the correlation function than is power law bias. To increase the small-scale correlations by more than a factor ~ 3 requires very severe thresholding in which galaxies only form in the very densest of environments.

A3 Cen-Ostriker bias

A final example which is amenable to analytical treatment is the case considered by Cen & Ostriker (1992), where there is a quadratic relationship between the logarithms of the light and mass densities:

$$\ln(\rho_g/\bar{\rho}_g) = C_0 + C_1 \ln(\rho_m/\bar{\rho}_m) + C_2 [\ln(\rho_m/\bar{\rho}_m)]^2. \quad (\text{A14})$$

Note that for $C_2 = 0$, this is just the earlier power law model, and that the maximum value for C_2 is $1/2\sigma^2$, as the mean density diverges if that limited is exceeded. If the density field is lognormal, then the properly normalized version of this becomes

$$1 + \delta' = \sqrt{1 - 2C_2\sigma^2}$$

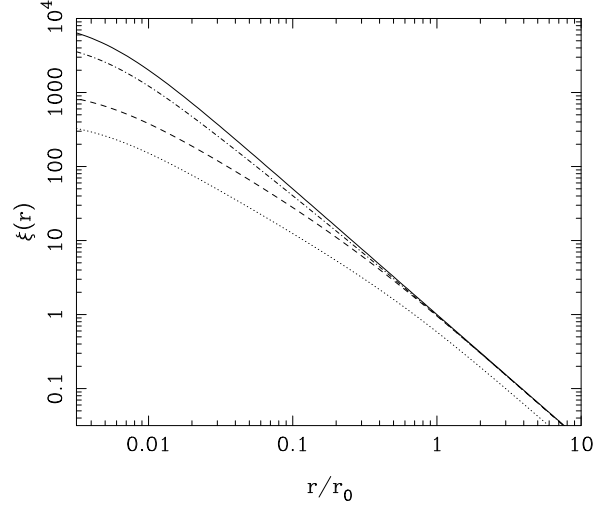


Figure A1. A plot of various correlation functions. The dotted line shows ξ for the mass, set so that pure power law bias with $B = 1.23$ produces ξ' which is a reasonable match to observed galaxy clustering ($\gamma = 1.7$, with clustering extending up to $\xi = 10^4$). The three models shown all have the same linear $b_\infty = 1.23$. In order of increasing ξ' , they are (1) censoring only, rejecting 36 per cent of the mass; (2) censoring 12 per cent of the mass and power law bias with $B = 1.18$; (3) $B=1.23$ with no censoring.

$$\times \exp \left[(C_1 - C_2\sigma^2)\delta_G + C_2\delta_G^2 - \frac{(C_1 - C_2\sigma^2)^2\sigma^2}{2(1 - 2C_2\sigma^2)} \right]. \quad (\text{A15})$$

The integral for ξ' can be performed in this case, giving

$$1 + \xi' = \frac{(1 - 2C_2\sigma^2)\sqrt{1 - r^2}}{\sqrt{[1 - 2C_2\sigma^2(1 - r^2)]^2 - r^2}} \times \exp \left[\frac{(C_1 - C_2\sigma^2)^2\sigma^2 r}{1 - 2C_2\sigma^2(2 + r) + 4C_2^2\sigma^4(1 + r)} \right]. \quad (\text{A16})$$

This has the linear bias

$$b_{\text{LN}} = \frac{C_1 - C_2\sigma^2}{1 - 2C_2\sigma^2}, \quad (\text{A17})$$

which gives the power law case when $C_2 = 0$. However, we also see that the bias is weakened when C_2 is negative, so that the light density is suppressed at extreme overdensity: the linear bias is unity when

$$C_2 = C_{2,\text{crit}} = -(C_1 - 1)/\sigma^2. \quad (\text{A18})$$

This paper has been produced using the Royal Astronomical Society/Blackwell Science L^AT_EX style file.